# Influence of Polymer Architecture on the Formation of Micelles of Miktoarm Star Copolymers Polyethylene/ Poly(ethylenepropylene) in the Selective Solvent Decane

**A. Ramzi,[†] M. Prager,* and D. Richter**

*Institut für Festkörperforschung, Forschungszentrum Jülich, D-52425 Jülich, Germany*

**V. Efstratiadis and N. Hadjichristidis**

*Department of Chemistry, University of Athens, Athens 15771, Greece*

**R. N. Young and J. B. Allgaier[‡]**

*Department of Chemistry, University of Sheffield, Sheffield S3 7HF, U.K.*

*Received January 14, 1997; Revised Manuscript Received July 2, 1997[⊗]*

ABSTRACT: Aggregates composed of branched polymers of the type $PE_nPEP_m$ ($n$, $m = 1, 2$ with $m + n = 3,4$), called *miktoarm stars*, in the selective solvent decane were investigated by small-angle neutron scattering using the contrast variation technique. The PE (polyethylene) arms were about 75% deuterated and of fixed molecular weight (7300), while the PEP [poly(ethylenepropylene)] chains were completely protonated and had molecular weights of 4900, 9100, and 15 700. The crystallization following the segregation of PE in decane drives the assembly process. As in the case of diblock copolymers PE−PEP, the miktoarm stars form lamellar structures with a flat dense crystalline PE core and a soft corona of PEP hairs sticking out on both sides of the core. Laterally, the aggregates are largely extended and modeled as thin disks. The densities of both the core and the corona were represented by step functions convoluted with a Gaussian each. The structural parameters (the thickness of the core and the extension of the hairs) were extracted using a model fitting. With increasing the PEP molecular weight, the average extension of the PEP chains in the corona increases and the thickness of the core decreases except for the symmetric architecture $PE_2$ $PEP_2$. The changes are different from those expected from an equivalent increase of molecular weights in a diblock. At room temperature almost all the polymer is found in the micelles. Thus, a thermodynamic description is based on the free energy of a single micelle. It yields scaling relations dependent on the star architecture. While the model worked well for the diblocks, it does not describe the core thickness variation correctly for the miktoarm systems.

## 1. Introduction

It is well known that a block copolymer of A−B type dissolved in a selective solvent which is thermodynamically a good solvent for one of the blocks and a precipitant for the other may associate to aggregates (lamellae, spheres, cylinders, etc.) as a result of the unsolubility of one of the copolymer blocks. Such aggregates consist of a relatively compact *core* formed by the least soluble blocks surrounded by a flexible and highly swollen brush (corona) formed by the other block.[1−3] Many techniques have been used to investigate the aggregation phenomena such as small-angle neutron scattering (SANS),[4] small-angle X-ray scattering,[5,6] low-angle and dynamic light scattering,[7−10] and viscosimetry.[11,12]

For the vast majority of A−B type block copolymers which have been studied to date, the domain diameters for spheres and cylinders and the thicknesses of lamellae fall within the range 50−1000 Å. However, the length of cylindrical domains and the breadth and length of the lamellae can approach macroscopic dimensions in samples where the morphology is well developed.

The factors that influence the aggregation process and the structural parameters of the aggregates include composition, molecular weight of the copolymer, architecture, interactions between the copolymer blocks and the solvent, copolymer concentration, temperature, and—in unfavorable systems out of equilibrium—the preparation method. Many studies on the characterization of aggregates in solution have been carried out in recent years. However, few of them have paid attention to the effect of the length of the copolymer block and polymer architecture on the aggregation number and dimensions of the aggregates and the thermodynamic behavior of dilute solutions of blocks A−B copolymers.

Samples of relatively homogeneous A−B systems, in which one block crystallizes, often show a domain morphology consisting of alternating crystalline and amorphous layers, with the chemical bond connecting the two parts of the copolymer lying in the interfacial regions between the layers.[13−16] This is schematically outlined in Figure 1a. The immiscible core blocks are shown to undergo chain-fold crystallization. However, other structures are possible depending on the crystallization conditions and the structure of the crystallizing blocks.[17,18] Thermodynamically, the equilibrium structure of the aggregates is controlled by the balance of the core's surface free energy and the deformation of the disordered flexible coronal blocks.[19−21]

The aggregation of polyethylene−poly(ethylenepropylene) (PE−PEP) block copolymers dissolved in decane was studied by SANS recently.[22−24] Richter et al.[22,24] found the systems to have a very low critical micelle concentration. Thus, at the concentrations studied all polymers are precipitated in lamellar micelles with a crystalline PE core and a corona of PEP hairs. The density profiles of both the core and the

[†] Present address: DSM Research, P.O. Box 18, PAC Department, NL-6160 MD Geleen, The Netherlands.

[‡] Present address: Institut für Festkörperforschung, Forschungszentrum Jülich, D-52425 Jülich, Germany.

[⊗] Abstract published in *Advance ACS Abstracts,* November 1, 1997.

S0024-9297(97)00038-7 CCC: $14.00 

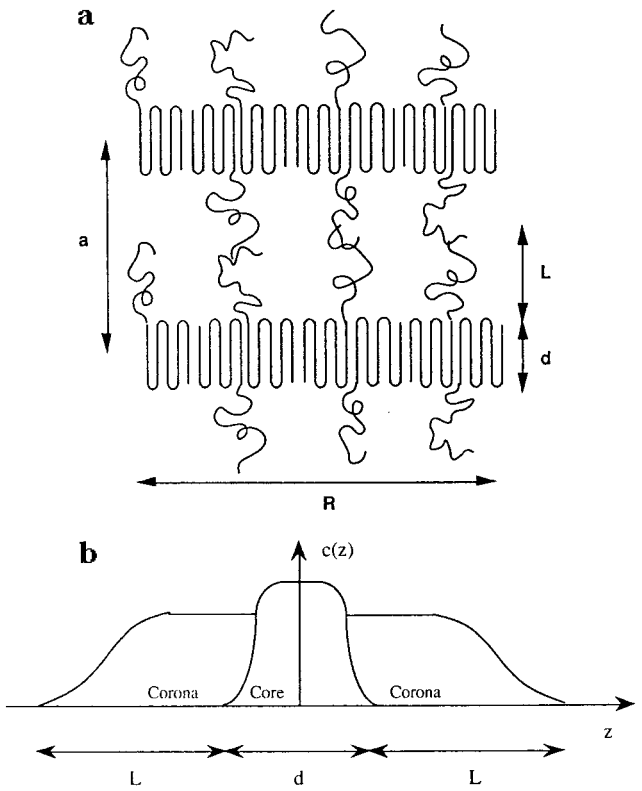


**Figure 1.** (a) Schematic outline of microphase separation in an A−B block copolymer in which one component is crystalline; *d* and *L* are the thicknesses of the lamellae domains (the core thickness and corona extension). (b) Density distribution (density profile) of A and B segments in A−B block copolymers, perpendicular to one platelet, exhibiting microphase separation.

brush were taken constant in their regime and convoluted with a Gaussian. The latter is done to account for smearing effects and to interpolate smoothly between two different theoretical predictions, using alternatively either a step[25,26] or a parabolic[27] density profile of the corona. The experimental data could be well fitted by a profile resembling the parabola. The variation of the structural parameters of the brushes followed scaling relations obtained from an analysis of the free energy of a single micelle. The lamellae were found to aggregate to stacks. Shear experiments allowed one to order the system over macroscopic dimensions. It could be shown that the van der Waals interaction between the large lamellae overcomes, at short intermicellar distances, the loss of translational entropy connected with the micellar aggregation.

The aim of the present paper is to study the influence of polymer architecture on the micelle formation. For this purpose instead of linear diblocks miktoarm star polymers (mikto comes from the Greek word *μικτοζ* meaning mixed) with a functionality of the center ≤4 are used. This allows the preparation of a series of polymers $PE_nPEP_m$ ($n$, $m = 1$, 2 with $m + n = 3,4$). Like in the previous study of diblocks, decane is used as the selective solvent. The investigation is carried out as a function of the molecular weight of the PEP arms while the length of the PE arms is kept constant. It was expected, and is confirmed below, that the architecture does not modify the global shape of the micelle but only its geometrical parameters.

The interest in the PE−PEP system is partly due to its possible technical potential as viscosity modifier, as suppresser of waxing in diesel fuel, and as hot melt adhesive. The first two of these applications are based on the aggregation behavior of these materials as a function of temperature, the composition of the solvent, and the selective miscibility of polymers in general.

## 2. Experimental Section

**2.1. Samples.** The miktoarm star copolymers of the $(PE)_n(PEP)_m$ type ($n$, $m = 1,2$, $n + m = 3,4$) were obtained by hydrogenation of the corresponding copolymers of deuterated polybutadiene (d-PB) and polyisoprene (PI). The hydrogenation was carried out with $Pd/CaCO_3$ (Pd: 5 wt %) catalyst in a 1 wt % polymer solution in heptane (polymer: catalyst, 1:1) at 80−100 °C and ∼36 bar for 24 h.[28] $^1$H-NMR confirmed the absence of the double bond signals. However, we notice here that because PB is deuterated the bond signals are due to only the PI part. Consequently, the absence of double bonds means that the PI part is fully saturated. Taking into account that hydrogenation of d-PB is easier than that of PI,[28] we conclude that the materials are fully saturated.

The synthesis of $(d\text{-}PB)_n(PI)_m$ was performed by anionic polymerization and controlled chlorosilane chemistry, using high vacuum techniques in evacuated, butyllithium (*n*-BuLi) washed, and benzene-rinsed glass reactors. Addition of the reagents was made through break-seals and removals of aliquots for characterization by heat sealing constrictions. Details on the reagent purification and linking reactions are described elsewhere.[29] *sec*-BuLi, prepared from *sec*-butyl chloride and lithium dispersion, was the initiator and benzene the solvent for all polymerizations.

Hypothetically, the synthesis of $A_n B_m$ ($n = 1,2$, $n + m = 3,4$) miktoarm stars containing PB and PI arms could be accomplished directly by using the appropriate amount of living polydienes and chlorosilane. For the synthesis of $(PI)_2(PB)$, the general reaction scheme is the following (Me: $CH_3$):

$$2PILi + MeSiCl_3 \rightarrow (PI)_2SiMeCl + 2LiCl$$

$$(PI)_2SiMeCl + \text{excess } PBLi \rightarrow (PI)_2SiMe(PB) + LiCl$$

However, both PILi and PBLi living chain ends are very reactive toward the chlorosilane. Some three-arm star $(PI)_3SiMe$ is also formed due to the small difference in reactivity between the substitution of the second and third chlorine atoms. One potential means of preventing substitution of the third chlorine atom is to cap the PI living chain with 2−3 units of a moderated bulky monomer, i.e., styrene (S). Thus, the basic reactions for the synthesis of $(PI)_2$ (d-PB) finally used are

$$PILi + \text{styrene} \rightarrow PIS_{2-3}Li$$

$$2PIS_{2-3}Li + MeSiCl_3 \rightarrow (PIS_{2-3})_2\,SiMeCl + 2LiCl$$

$$(PIS_{2-3})_2SiMeCl + \text{excess d-PBLi} \rightarrow (PIS_{2-3})_2SiMe(\text{d-PB}) + LiCl$$

The same method was used for the synthesis of $(PI)_2$ $(d\text{-}PB)_2$ miktoarm stars using $SiCl_4$ instead of $MeSiCl_3$.[30]

In the case of $(PI)(d\text{-}PB)_2$ materials, the capping of PILi was done with diphenylethylene (DPE), a monomer bulkier than styrene, in order to substitute only one chlorine atom. In this case only one unit is added to the living PI. The following reaction scheme was used:

$$PILi + DPE \rightarrow PI(DPE)Li$$

$$PI(DPE)Li + MeSiCl_3 \rightarrow PI(DPE)SiMeCl_2 + LiCl$$

$$PI(DPE)SiMeCl_2 + \text{excess d-PBLi} \rightarrow PI(DPE)SiMe(\text{d-PB})_2 + 2LiCl$$

**Table 1. Characteristics of the Different Miktoarm Copolymers before Hydrogenation[a]**

| system | sample[b] | VPO $M_{n(PI)}$ | VPO $M_{n(d-PB)}$ | $M_{n(star)}$ MO | $M_{w(star)}$ (LALLS) | $I$ (SEC) | $M_{n(star)}$ (calcd) | $N_{PE}$ | $N_{PEP}$ |
|---|---|---|---|---|---|---|---|---|---|
| | MAS522 | 4800 | 7100 | 18 500 | 19 600 | 1.05 | 19 000 | 118 | 71 |
| $(d\text{-}PB)_2(PI)_2$ | MAS822 | 8900 | 6900 | 20 600 | 22 000 | 1.05 | 21 700 | 115 | 131 |
| | MAS152 | 15200 | 6800 | 29 000 | 30 100 | 1.04 | 28 800 | 113 | 224 |
| | MAS512 | 4800 | 7100 | 16 200 | 17 000 | 1.04 | 16 700 | 118 | 71 |
| $(d\text{-}PB)(PI)_2$ | MAS812 | 8900 | 6400 | 23 300 | 24 500 | 1.05 | 24 200 | 107 | 131 |
| | MAS1512 | 15200 | 6800 | 37 400 | 38 300 | 1.04 | 37 200 | 113 | 224 |
| | MAS521 | 4800 | 7300 | 24 100 | 25 200 | 1.03 | 24 200 | 122 | 71 |
| $(d\text{-}PB)_2(PI)$ | MAS821 | 8600 | 7300 | 32 500 | 34 400 | 1.05 | 31 800 | 122 | 126 |
| | MAS152 | 14900 | 6900 | 42 300 | 44 000 | 1.04 | 43 000 | 115 | 219 |

[a] Techniques used: VPO = vapor-pressure osmometry. MO = membrane osmometry. LALLS = low-angle laser light scattering. SEC = size-exclusion chromatography. $N_{PE}$, $N_{PEP}$: number of monomers in a single polymer arm. [b] Name of sample used after hydrogenation.

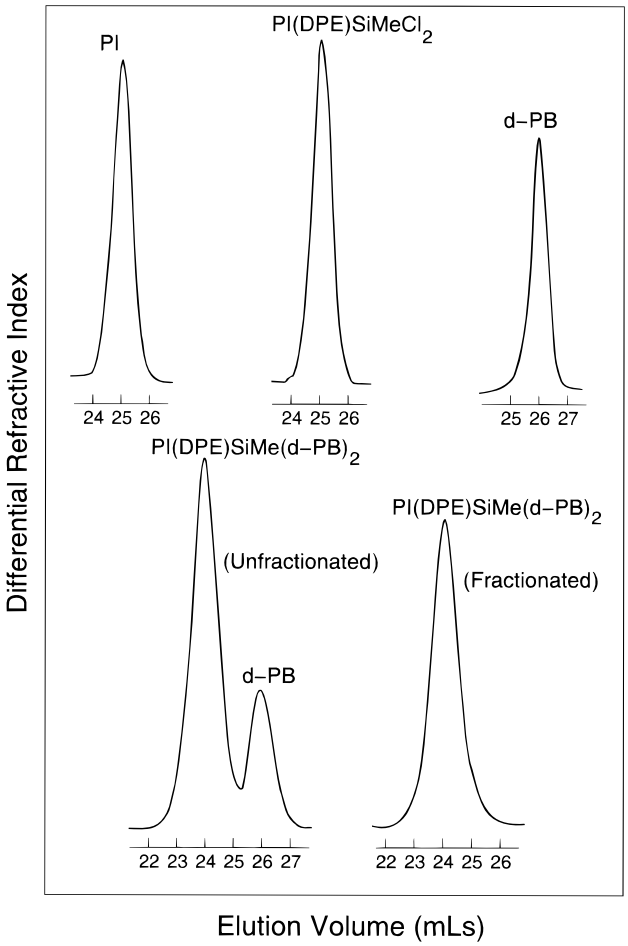


**Figure 2.** SEC traces taken during the synthesis of one three-miktoarm star copolymer of the $(PI)(d\text{-}PB)_2$ type.

All steps of linking reactions were monitored by size exclusion chromotography (SEC). A typical example is given in Figure 2. The fractionation of the linking reaction product was carried out by adding methanol to the polymer solution (1 wt %) in toluene at room temperature. It was performed until no precursors were shown to be present by SEC.

The molecular weight of PE was kept about constant while that of PEP was varied. To characterize the polymers, SEC (THF, 30 °C), low-angle laser light scattering (LALLS; THF, 25 °C), laser differential refractometry (THF, 25 °C), membrane osmometry (MO; toluene, 35 °C), vapor-pressure osmometry (VPO; toluene, 50 °C), and $^1$H- and $^{13}$C-NMR ($CDCl_3$, 30 °C) measurements were performed following procedures published elsewhere.[29,31] The molecular characteristics given in Table 1 indicate a high degree of molecular and compositional homogeneity. In addition, the composition calculated from the $M_n$ of arms was found to be in agreement with that obtained by NMR. The dienic precursors analyzed by NMR were found to have the typical microstructure corresponding to PB and PI obtained in benzene by *sec*-BuLi.[32]

The miktoarm stars of composition $(PE)_n(PEP)_m$ ($n$, $m = 1$, 2 with $m + n = 3$, 4) were obtained starting from the described (PB)−(PI) stars by subsequent hydrogenation.

Protonated PI and deuterated PB arms, respectively, were used to have a contrast in neutron scattering experiments. After hydrogenation of the double bonds, the PI arms transform to a fully hydrogenated PEP polymer, whereas the PB arms become partially deuterated PE having ideally a structure $C_4D_{8(1-y)}H_{8y}$ with $y = 0.25$. For this $y$-value any double bond picks up exactly one proton.

In ref 33 the fractional substitution $y$ of hydrogen in PE made from d-PB has been determined experimentally. The obtained values of $y$ exceed the ideal value $y = 0.25$ significantly due to a stimulated H−D exchange during the hydrogenation reaction. This observation has been confirmed for our samples by evaluating quantitatively the SANS intensities of identical samples measured at various contrasts.[24] A consistent description was obtained for a composition $C_4D_{4.8}H_{3.2}$. Very closely related and well within the error bars of this experiment, $y = 0.375$ was chosen in this work.

Furthermore, the densities in the various subunits of the aggregate play an important role when calibrating SANS data (see below). Many authors have studied the density of crystalline PE. It was found that the theoretical value of 1.00 g/cm$^3$, calculated from the dimensions of the unit cell of a PE crystal, is never reached in practice.[33−35] This is especially true for PE synthesized by hydrogenation of PB. Here the density depends seriously on the number of ethylene side chains per skeletal carbon and can be estimated to $\zeta_{PE} = 0.93 \pm 0.02$ g/cm$^3$.[34] The density of PEP is well known to be $\zeta_{PEP} = 0.856$ g/cm$^3$.

In order to get samples in thermodynamical equilibrium, the polymers were dissolved in decane at a temperature of 60 °C, which is higher than the melting temperature of the crystalline PE lamellae in the micelle. The solution is then transparent. By cooling slowly down to room temperature, the solution may, depending on the concentration, the molecular weight of the star, and the architecture, become more and more opaque, indicating the formation of aggregates.

**2.2. Small-Angle Neutron Scattering.** Small-angle neutron scattering experiments (SANS) were performed at the spectrometers PACE at the Laboratoire Léon Brillouin (LLB) in Saclay, France, at D11 at the Institut Laue-Langevin (ILL) in Grenoble, France, and at KWS1 at the Institut für Festkörperforsching (IFF), KFA Jülich, Germany. This experimental technique has been described elsewhere.[36−38] Data were taken at different configurations of the spectrometers, i.e., different wavelengths $\lambda$ of the incident neutrons and different detector−sample distances corresponding to different angular resolution. The range of momentum transfer $Q = (4\pi/\lambda)\sin(\vartheta/2)$ ($\vartheta$: scattering angle) was $0.0008\ \text{Å}^{-1} \le Q \le 0.3\ \text{Å}^{-1}$.

The scattering was, in general, performed at room temperature. Some scans at higher temperature were aimed to show the critical micelle concentration. The data were radially averaged to reduce the statistical error. The scattering due to the empty cell and the solvent, as well as a calculated incoherent background caused by the protons, was subtracted. Thereafter, the neutron scattering intensity of the raw data

is normalized, with the scattering of 1 mm of water used as a standard. The water scattering was also used to determine the detector efficiencies. Finally, *after normalization to the concentration*, one obtains the coherent scattering cross section $d\Sigma(Q)/d\Omega$ in absolute units.

## 3. Scattering from Solutions of PE−PEP Platelets: Model Fitting

In this paragraph, we introduce the theoretical basis to describe the experimental data and extract the structural parameters characterizing the aggregates. Lead by the crystallization behaviour of PE and the successful description by lamellar brushes in the earlier paper on block copolymers,[22,24] form factors of disklike aggregates were successfully used to describe the observed scattering patterns. The thin disk is characterized by a radius $R$, a thickness $d$ of the crystalline core, and a soft corona of length $L$ of PEP hairs sticking out of both sides of the core (Figure 1a). We first calculate the scattering amplitude and the intensity of one single oriented platelet and then average over the possible orientations of the surface of the platelet.

**3.1. Contribution of the Average Density Profile.** The scattering amplitude is the Fourier transform of the density profile $c(\mathbf{r})$ weighted by the contrast factor $\Delta\rho$

$$A(\mathbf{Q}) = \Delta\rho \int c(\mathbf{r})\, e^{i\mathbf{Q}\mathbf{r}}\, d\mathbf{r} \tag{1}$$

For a planar system, infinitely extended laterally, the scattering is reduced to the direction $z$ perpendicular to the surface. Therefore, the scattering amplitude becomes

$$A(Q_\perp) = \Delta\rho \int c(z)\, e^{iQ_\perp z}\, dz \tag{2}$$

The scattering intensity of a disk of finite lateral dimension $R$ averaged over all orientations can be expressed as[39]

$$I(Q) = \int_0^{\pi/2} |A(Q\cos\vartheta)^2 \left|\frac{2\pi R^2 J_1(QR\sin\vartheta)}{QR\sin\vartheta}\right|^2 \sin\vartheta\, d\vartheta \tag{3}$$

where $J_1$ is the cylindrical Bessel function of the first order. In the case $R \gg d$ ($d$: thickness of the disk), this equation can be approximated as

$$I(Q) = (2\pi R^2)^2 |A(Q)|^2 \int_0^{\pi/2} \left|\frac{J_1(QR\sin\vartheta)}{QR\sin\vartheta}\right|^2 \sin\vartheta\, d\vartheta \tag{4}$$

By approximating

$$\left|\frac{J_1(QR\sin\vartheta)}{QR\sin\vartheta}\right|^2 \approx \frac{1}{4}\exp\left(-\left(\frac{QR\sin\vartheta}{2}\right)^2\right) \tag{5}$$

the scattering intensity can be cast into the form

$$I(Q) = (\pi R^2)^2 |A(Q)|^2 \frac{D\left(\frac{QR}{2}\right)}{\frac{QR}{2}} \tag{6}$$

where $D$ is the Dawson function given by

$$D(u) = \exp(-u^2)\int_0^u \exp(t^2)\, dt \tag{7}$$

For the brush profile many different theoretical predictions covering the range from an exact step profile,[25] a combination between power law and step profile,[26] and a parabolic profile[27] were proposed. A mathematical expression of the profile was chosen which, depending on its parameters, can closely approximate any of these model densities. It consists of a rectangular profile for the core and the corona convoluted with a Gaussian each (Figure 1b). The corresponding scattering amplitude can be easily calculated.

Due to the presence of two substructures the scattering amplitude is

$$A(Q) = A^c(Q) + A^b(Q) \tag{8}$$

with

$$A^c(Q) = \Delta\rho_c d \frac{\sin(Qx)}{Qx} \exp\left(\frac{-Q^2\sigma_d^2}{2}\right) \tag{9}$$

$$A^b(Q) = \Delta\rho_b \frac{cd}{L}\left[2y\frac{\sin(Qy)}{Qy}\exp\left(\frac{-Q^2\sigma_L^2}{2}\right) - d\frac{\sin(Qx)}{Qx}\exp\left(\frac{-Q^2\sigma_d^2}{2}\right)\right]$$

Here $x = d/2$ and $y = L + d/2$ with $L$ the extension of the PEP arms (brush length). $\sigma_d$ and $\sigma_L$ are the smearing parameters of the core and the brush, respectively. The scattering of the brush must take into account the PEP fraction only. This is the effect of the geometric factor $cd/L$ with $c = \zeta_{PE}M_{PEP}/2\zeta_{PEP}M_{PE}$. The scattering length density $\Delta\rho_c$ is calculated under the assumption that there is no solvent in the core.

The finally important quantity is the coherent scattering cross section per unit volume which is related to $I(Q)$ by

$$\frac{d\Sigma(Q)}{d\Omega} = \Phi\frac{\Phi_{PE}}{V_{PE}} I(Q) \tag{10}$$

Here $\Phi$ is the total polymer volume fraction, $\Phi_{PE}$ the relative fraction of PE in the miktoarm star, and $V_{PE} = \pi R^2 d$ the volume of the PE core.

**3.2. Structure Factor due to Micellar Aggregation and Contribution of the Concentration Fluctuations.** There are two further effects which modify this expression. First, outlined in the introduction, the platelets aggregate to stacks by van der Waals interaction.[22] This leads to a structure factor $S(Q)$ which essentially represents the platelet center-of-mass correlation function. Second, the brush is not really homogeneous as assumed so far but shows density fluctuations. Coherency is maintained only in a finite volume called a *blob*, while the scattering from different blobs is incoherent. This adds a second term to the expression of the scattering intensity. Thus, the combined scattering of the average density profile and the blobs yields

$$\frac{d\Sigma(Q)}{d\Omega} = \Phi\frac{\Phi_{PE}}{V_{PE}} I(Q)\, S(Q) + \frac{d\Sigma^b(Q)}{d\Omega} \tag{11}$$

We first consider the structure factor $S(Q)$ of a stack of parallel platelets with a distribution of the interplatelet distances. It is known as the *paracrystal*

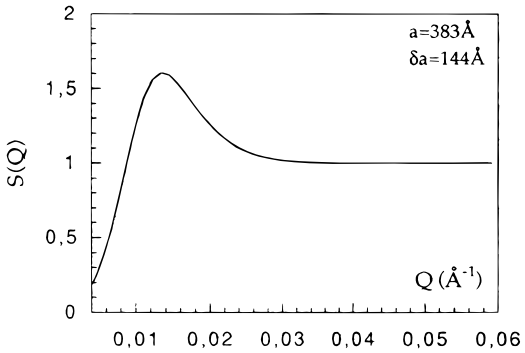


**Figure 3.** Calculated structure factor $S(Q)$ taking a stacking period $a = 383$ Å and a distance distribution $\delta a = 144$ Å.

structure factor[40] and has for a Gaussian type distribution of distances the form

$$S(Q) = \frac{\exp\left(\frac{\delta a^2 Q^2}{2}\right) - 1}{\exp\left(\frac{\delta a^2 Q^2}{2}\right) + 1 - 2\cos(Qa)\exp\left(\frac{\delta a^2 Q^2}{4}\right)} \quad (12)$$

The parameter $a$ is the average distance between platelets and $\delta a$ is the distance fluctuation (Figure 3). Due to the rather large value of $a$, the effect of the structure factor is visible only at low $Q \leq 2\pi/a$, while it approaches unity at higher $Q$. Note also that the limit at $Q \rightarrow 0$ is

$$S(Q\rightarrow 0) = \frac{\delta a^2}{2a^2} + \left(\frac{\delta a^2}{24} - \frac{\delta a^6}{32a^4}\right)Q^2 + 0(Q^4) \quad (13)$$

which corresponds to a marked correlation hole at small $Q$. For finite stacking $NP$, however, the forward scattering is again enhanced when the momentum transfer reaches $Q \sim 2\pi/(NP)a$ with $(NP)a$ the dimension of the macroaggregates.

The blob scattering is calculated in ref 41. An ensemble of blobs of average size $\xi$ thus is characterized by the correlation function $G(r)$

$$G(r) \sim r^{1/\nu - 3}\exp(-r/\xi) \quad (14)$$

The Fourier transform of $G(r)$ leads to the blob scattering function

$$I^{\mathrm{b}}(Q) = \frac{\Delta\rho_{\mathrm{b}}{}^2 \times 4\pi\alpha\Gamma(\mu)\xi^{\mu}}{Q}\frac{\sin(\mu\tan^{-1}(Q\xi))}{(1+Q^2\xi^2)^{\mu/2}} \quad (15)$$

where $\mu = 1/\nu - 1$, $\Gamma(\mu)$ is the gamma function with argument $\mu$, and $\alpha$ is a constant to be determined.

As shown in ref 20, the blob scattering in the brush $\mathrm{d}\Sigma^{\mathrm{b}}(Q)/\mathrm{d}\Omega$ can be written for blobs of constant size and density as

$$\begin{aligned}\mathrm{d}\Sigma^{\mathrm{b}}(Q)/\mathrm{d}\Omega &= \Phi\frac{\Phi_{\mathrm{PEP}}}{V_{\mathrm{blob}}}I^{\mathrm{b}}(Q)\\ &= \Delta\rho_{\mathrm{b}}{}^2\Phi\Phi_{\mathrm{PEP}}\xi^3\frac{1}{\mu}c\frac{d}{L}\frac{1}{Q\xi}\frac{\sin(\mu\tan^{-1}(Q\xi))}{(1+Q^2\xi^2)^{\mu/2}}\end{aligned} \quad (16)$$

Here again $\Phi$ is the total polymer volume fraction and $\Phi_{\mathrm{PEP}}$ denotes the relative fraction of the PEP part in the miktoarm star.

The blob diameter is related to the grafting density of the PEP hairs. The area $\xi^2$ per PEP arm determines the size $\xi^3$ of the blob. It is thus related to the core thickness and the polymer architecture according to

$$\xi = \left(\frac{2M_{\mathrm{PE}}}{N_{\mathrm{a}}\zeta_{\mathrm{PE}}d}\right)^{1/2}\left(\frac{I_{\mathrm{PE}}}{I_{\mathrm{PEP}}}\right)^{1/2} \quad (17)$$

with Avogadro's number $N_a$, the molecular weight of one PE arm, $M_{\mathrm{PE}}$, and the density of the PE, $\zeta_{\mathrm{PE}}$. The effect of the architecture is introduced via the factor $I_{\mathrm{PE}}/I_{\mathrm{PEP}}$ where $I_{\mathrm{PE}}$ and $I_{\mathrm{PEP}}$ represent the numbers of PE and PEP arms, respectively.

The equation of the scattering cross section with all the factors derived above contains terms which are of importance in different $Q$ regimes. For small $Q$, the scattering relates to the stacking of platelets, at intermediate $Q$ it is dominated by the average density profile in the core and the brush. For large $Q$, the scattering is like the large-angle scattering from a semidilute polymer solution, i.e., it represents the scattering from a power law density correlation function with the power $1/\nu$.

In order to compare the measured data to the calculated scattering patterns, the results of eq 11 are convoluted by a Gaussian type instrumental resolution function, taking into account experimental parameters like wavelength spread, collimation and detector resolution according to Pedersen et al.[42]

## 4. Results

**4.1. Concentration Dependence.** In order to estimate the importance of interaction between aggregates we studied the systems at different concentrations in the range $0.25\% \leq \Phi \leq 3\%$ in brush contrast. At such a condition, the obtained spectra correspond mostly to the PEP phase in the aggregate. The measurements were carried out at room temperature. Parts a and b of Figure 4 show the concentration dependence of SANS intensities from MAS822 and MAS1522 samples. These two samples were measured at momentum transfers $0.003\ \text{Å}^{-1} \leq Q \leq 0.12\ \text{Å}^{-1}$ and $0.0008\ \text{Å}^{-1} \leq Q \leq 0.3\ \text{Å}^{-1}$, respectively. The scattering patterns were normalized to the concentration in order to allow a direct comparison. At intermediate and high $Q$, they were found to be independent of the concentration as they collapse to a single curve. Similarly at low $Q$, the intensities look also independent of the concentration. Effects of the concentration on the structure factor obviously are absent.

The distinctive shape of the intensity from the brush is evident. While the linear polymer in solution is characterized by just one parameter, which is the radius of gyration (dilute solution) or the blob radius (semidilute solution), there are further characteristic lengths present in the brush. Even in dilute solution, the brush can be thought of as a region of semidilute polymer solution surrounded by pure solvent. Hence, the scattering at low momentum transfers $Q$ will essentially look like the scattering from particles with a size given by the size of the aggregate, while at high $Q$ the scattering will look like that from a semidilute polymer solution with its characteristic power law decay in $\mathrm{d}\Sigma(Q)/\mathrm{d}\Omega$. The characteristic exponent will be $-1/\nu$, where $\nu$ is the Flory exponent. At $\Theta$ conditions, the polymer is represented by a nearly ideal random walk and $\nu = {}^1/_2$. For our case of a good solvent, one has $\nu = {}^3/_5$ (self-avoiding random walk) and the scattering varies as

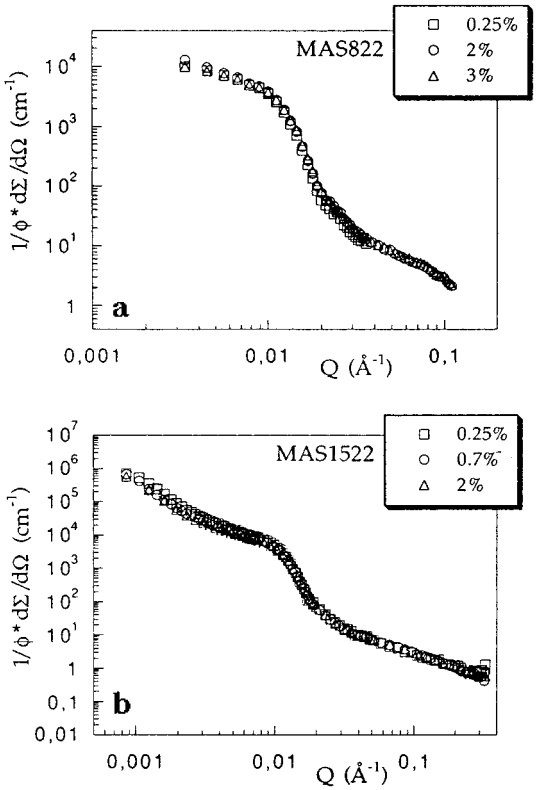


**Figure 4.** SANS data from samples (a) MAS822 and (b) MAS1522 at several total polymer concentrations. The solvent corresponds to the brush contrast.

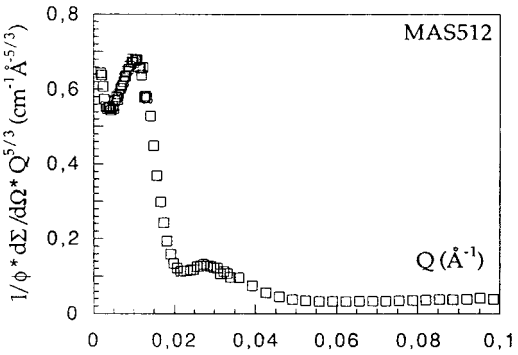


**Figure 5.** Generalized Kratky plot of SANS brush data for sample MAS512 at concentration 2% of polymer in decane.

$Q^{-5/3}$. In Figure 5 an example of the scattering spectra of the sample MAS512 is shown in a *generalized Kratky plot*. dΣ/dΩ was multiplied by $Q^{5/3}$ instead of $Q^2$. The flatness of the curve shows that this sample nicely exhibits the ideal self-avoiding chain behavior. For all the samples investigated in this paper, the exponent $\nu$ is found to vary between $^1/_2$ and $^3/_5$. Sometimes, in aggregates, this behavior is complicated by the stretching of the brush arms increasing with their molecular weight. Hence, the exponent $\nu$ is larger than $^3/_5$. Such a case was not observed in our samples.

The scattering patterns of the sample MAS522 (Figure 6) with the very short PEP arms are clearly different from those of identical architecture but longer PEP arms (Figure 4). In Figure 6 one distinguishes two domains: above $Q^* = 0.012$ Å$^{-1}$ the intensities are independent of concentration but show several oscillations. Below $Q^*$ we observe a systematic decrease of the intensity with increasing the concentration due to a more pronounced structure factor.

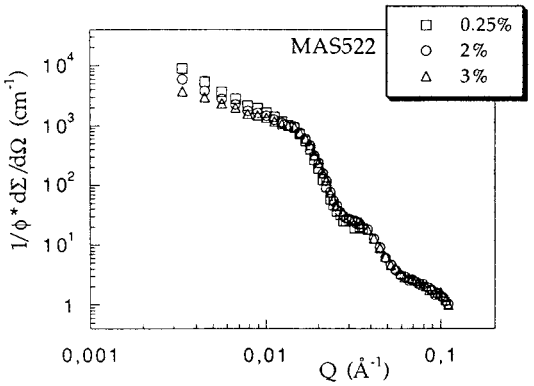


**Figure 6.** SANS data from sample MAS522 at several total polymer concentrations. The solvent corresponds to the brush contrast.

**Table 2. Parameters Obtained by Direct Model Fitting**

| sample | $d$ ($\sigma_d$)[a]/Å | $L$ ($\sigma_L$)[b]/Å | $L_p$[c]/Å | $a$ ($\delta a$)[d]/Å | $\xi$[e]/Å | $\xi$[f]/Å |
|---|---|---|---|---|---|---|
| MAS522 | 62 (16) | 105 (0) | 105 | 383 (144) | 27 | 16 |
| MAS822 | 59 (19) | 138 (57) | 205 | 536 (221) | 27 | 24 |
| MAS1522 | 60 (18) | 143 (83) | 245 | 578 (261) | 27 | 20 |
| MAS512 | 60 (18) | 151 (0) | 151 | 430 (170) | 15 | 20 |
| MAS812 | 49 (29) | 129 (52) | 205 | 470 (245) | 15 | 16 |
| MAS1512 | 50 (14) | 132 (130) | 313 | 579 (259) | 18 | 16 |
| MAS521 | 96 (40) | 99 (0) | 99 | 296 (131) | 30 | 24 |
| MAS821 | 83 (17) | 91 (53) | 155 | 444 (210) | 33 | 18 |
| MAS1521 | 40 (30) | 49 (125) | 265 | 562 (311) | 48 | 24 |

[a] Thickness and the smearing of the core. [b] Extension and the smearing of the brush. [c] Extension of the brush in the parabola description. [d] Distance between the platelets and their fluctuation. [e] Blob size values calculated using eq 17. [f] Blob size values extracted from the fit.

**4.2. Structure: Model Fitting and Partial Structure Factors.** The standard data analysis consists of a simultaneous fit of the spectra obtained for different contrasts to the platelet model according to eq 11. The SANS spectra are the Fourier transform of the scattering length density distribution in the sample. Thus, the global fit yields the geometrical parameters of the platelets: $d$, $\sigma_d$, $R$, $L$, $\sigma_L$, $a$, $\delta a$, $\alpha$, and $\xi$. We assumed the Flory exponent $\nu$ to be constant and equal to $^3/_5$. In spite of the best $Q$ resolution available in a neutron scattering experiment, no effect of the large $R$-values of our aggregates could be resolved. Thus, the lateral extension of the platelet $2R$ was fixed to a large value, 12 000 Å, which does not affect the calculated spectra in the measured $Q$ range. The scattering length density of the protonated PEP is taken as $\rho_{PEP} = -0.31 \times 10^{10}$ cm$^{-2}$, whereas the scattering length density of the PE chain is estimated from the fit to the value $\rho_{PE} = 4.871 \times 10^{10}$ cm$^{-2}$. This value is within experimental errors consistent with the results for diblocks, $(5.28 \pm 0.63) \times 10^{10}$ cm$^{-2}$,[22,24] and the value $4.70 \times 10^{10}$ cm$^{-2}$ proposed in ref 33. The fits for all samples are displayed as solid lines in Figures 7−9, and the results are listed in Table 2. The blob size $\xi$ may be estimated using the fit results based on either the expression for the blob scattering, eq 16, or eq 17, where $\xi$ is related to the mean distance between the PEP arms on the PE surface.

An alternative way of analysis is to extract from a set of data taken at different contrasts the different partial structure factors $S_{ij}$. The general expression for the cross section is

$$\frac{d\Sigma(Q)}{d\Omega} = \Delta\rho_b{}^2 S_{bb}(Q) + 2\Delta\rho_b\Delta\rho_c S_{bc}(Q) + \Delta\rho_c{}^2 S_{cc}(Q) \quad (18)$$

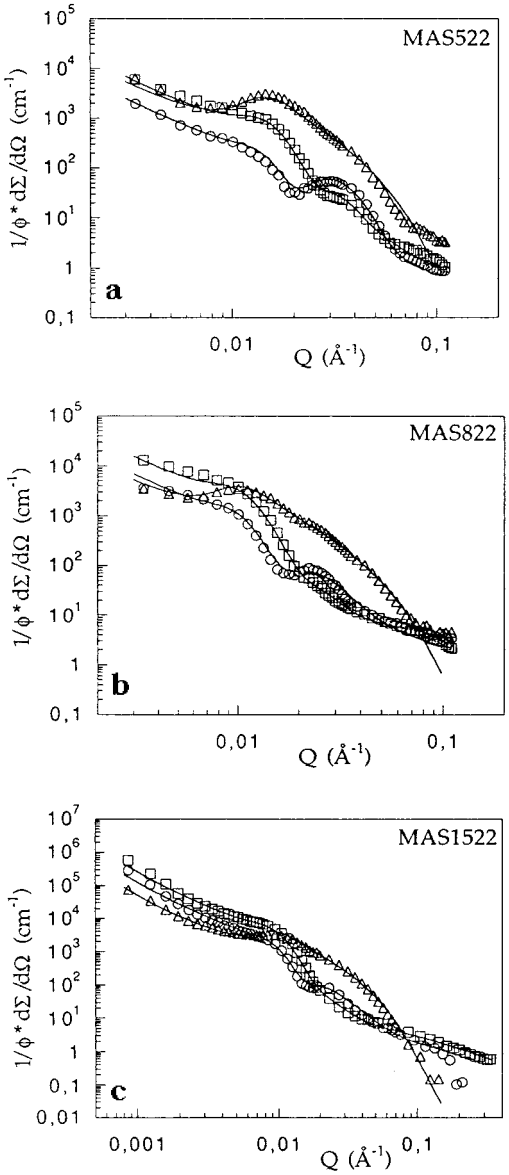


**Figure 7.** Contrast variation of the system with architecture $(PE)_2(PEP)_2$ at concentration 2% of polymer in decane in a double logarithmic representation: (a) MAS522, (b) MAS822, (c) MAS1522. The scattering length densities of the solvent are (□) $6.2 \times 10^{10}$, (○) $4.83 \times 10^{10}$, and (△) $-0.31 \times 10^{10}$ cm$^{-2}$. The solid lines represent the fit with the structural model.

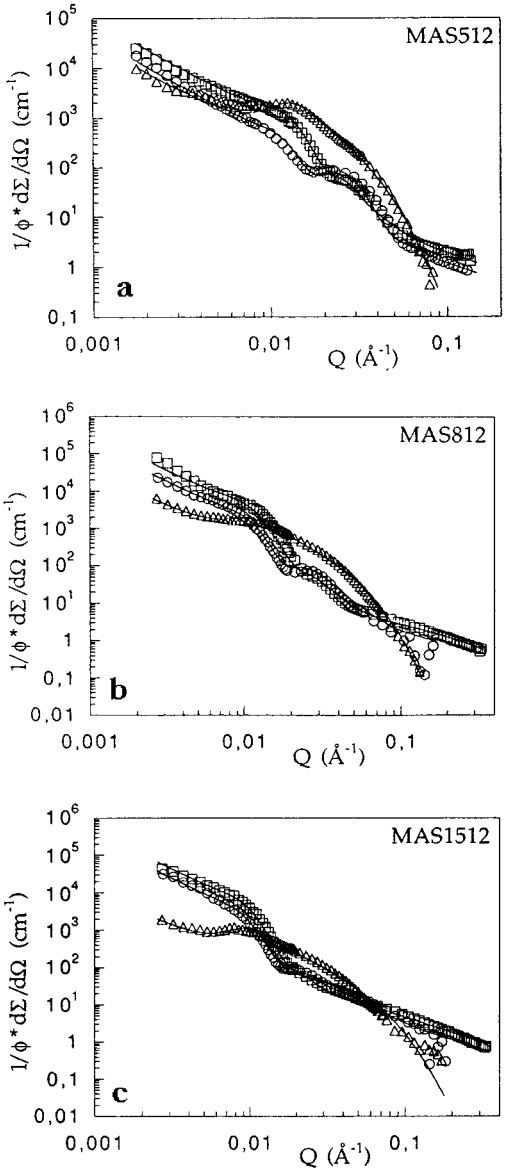


**Figure 8.** Contrast variation of the system with architecutre $(PE)(PEP)_2$ at concentration 2% of polymer in decane in a double logarithmic representation: (a) MAS512, (b) MAS812, (c) MAS1512. The scattering length densities of the solvent are (□) $6.2 \times 10^{10}$, (○) $4.83 \times 10^{10}$, (△) $-0.31 \times 10^{10}$ cm$^{-2}$. The solid lines represent the fit with the structural model.

where $\Delta\rho_b = \rho_b - \rho_s$ and $\Delta\rho_c = \rho_c - \rho_s$, with $\rho_b$, $\rho_c$, and $\rho_s$ are the respective scattering length densities of the polymer brush, the polymer core, and the solvent. The factors $\Delta\rho_i$ are the contrast factors between the polymer and the solvent.

There are three partial structure factors which describe in reciprocal space the brush−brush, $S_{bb}$, the brush−core, $S_{bc}$, and the core−core, $S_{cc}$, correlations. If three or more contrasts are measured, then the resulting system of linear equations (18) can be solved and the partial structure factors can be extracted. The mathematical procedure is described in more detail elsewhere.[22,24] Such a technique is useful to reduce the number of parameters entering the analysis of a single spectrum. For example, $S_{cc}$ contains only core parameters. The quantities $S_{ij}(Q)$ are defined as the Fourier transforms of the correlation function of the volume fractions of constituents i and j

$$S_{ij}(Q) = \int \langle \delta c_i(0)\, \delta c_j(\mathbf{r}) \rangle \exp(i\mathbf{Qr})\, d\mathbf{r} \qquad (19)$$

with i, j = b, c, or s. The term $\langle \delta c_i(0)\, \delta c_j(\mathbf{r}) \rangle$ is the density−density correlation function of the two phase medium.

In the experiment we have investigated all aggregates under four different contrast conditions at a concentration of 2%: contrast 1 allowed mainly the observation of the brush taking the pure deuterated decane as an almost matching solvent; contrast 2, based on an almost purely hydrogenous solvent, mainly revealed the scattering from the core. The problem was that due to uncertainties of the PE density and degree of hydration (see the Introduction) pure core or brush contrasts were not exactly obtained in the experiment. To complete the series, two further contrasts were measured. Note that the fourth contrast was used in order to increase the precision of the experimental data. In Figure 10 an example of the fitted partial structure factor of the core and the brush for the sample MAS1521 is presented on a double-logarithmic scale. Table 3 shows that both procedures yield very similar parameters.

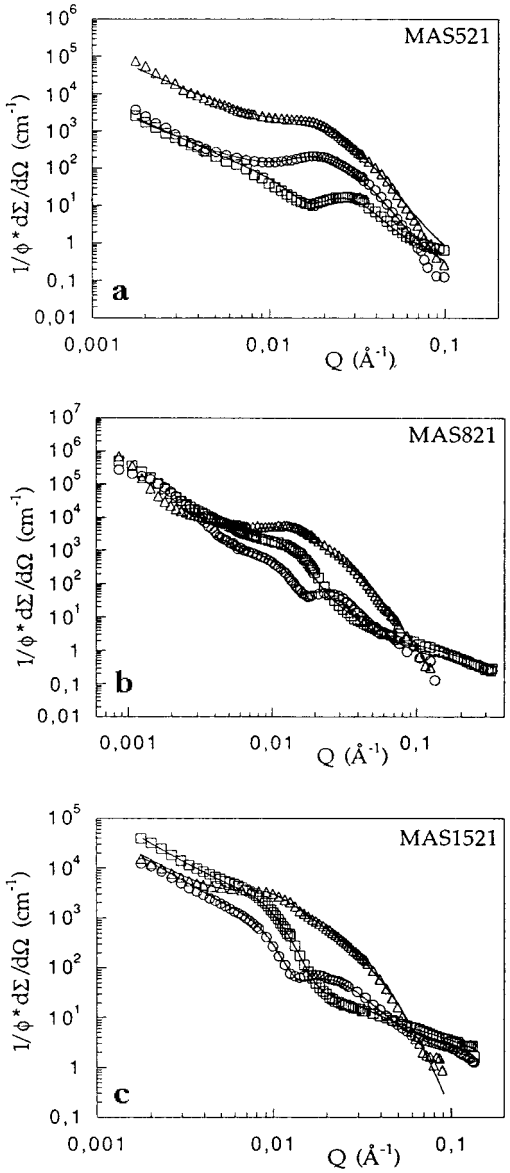


**Figure 9.** Contrast variation of the system with architecture $(PE)_2(PEP)$ at 2% concentration of polymer in decane in a double logarithmic representation. (a) MAS521, (b) MAS821, (c) MAS1521. The scattering length densities of the solvent are (□) $6.2 \times 10^{10}$, (○) $4.83\times10^{10}$, (△) $-0.31\times10^{10}$ cm$^{-2}$. The solid lines represent the fit with the structural model.

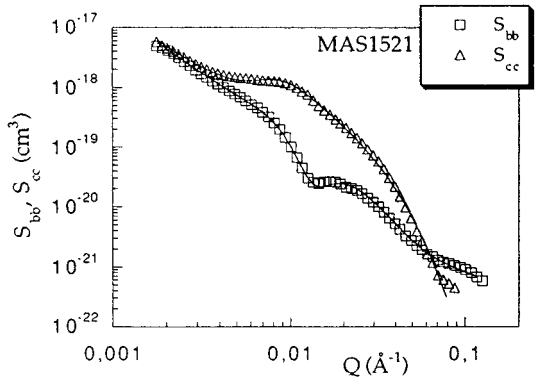


**Figure 10.** Partial scattering of the pure core $S_{cc}$ and pure brush $S_{bb}$ of sample MAS1521 at concentration 2% of polymer in decane extracted from eq 18, in a double-logarithmic representation. The solid lines represent the fit with the structural model.

In general, the aggregation process of block copolymers in a selective solvent is mainly determined by the total molecular weight of the block copolymer, the composition and likely the architecture. There exist certain limits with respect to composition and molecular weight, beyond which the block copolymers are insoluble.[7] For our PE/PEP systems, the aggregation is caused by the crystallization enthalpy of the PE component.

**Table 3. Parameters Obtained by Fitting Partial Structure Factors**

| sample | $d$ ($\sigma_d$)[a]/Å | $L$ ($\sigma_L$)[b]/Å | $a$ ($\delta a$)[c]/Å | $\xi^d$/Å | $\xi^e$/Å |
|---|---|---|---|---|---|
| MAS522 | 63 (16) | 106 (0) | 365 (144) | 27 | 16 |
| MAS822 | 54 (18) | 149 (55) | 547 (224) | 28 | 28 |
| MAS1522 | 59 (19) | 172 (73) | 574 (262) | 27 | 22 |
| MAS512 | 53 (29) | 150 (0) | 409 (165) | 14 | 20 |
| MAS812 | 49 (15) | 134 (68) | 467 (252) | 15 | 14 |
| MAS1512 | 39 (14) | 166 (119) | 561 (253) | 16 | 20 |
| MAS521 | 94 (40) | 104 (0) | 300 (128) | 30 | 26 |
| MAS821 | 84 (17) | 113 (64) | 469 (227) | 33 | 20 |
| MAS1521 | 39 (31) | 47 (127) | 581 (303) | 48 | 22 |

[a] Thickness and the smearing of the core. [b] Extension and the smearing of the brush. [c] Distance between the platelets and their fluctuation. [d] Blob size values calculated using eq 17. [e] Blob size values extracted from the fit.

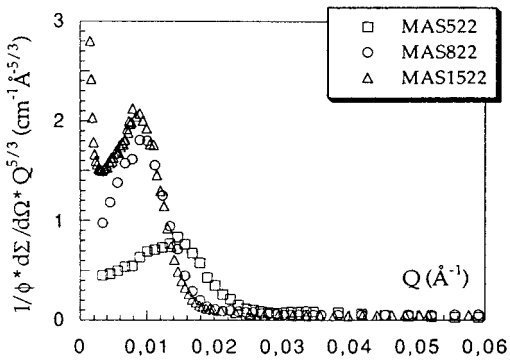


**Figure 11.** Scattering cross section for the samples with architecture $(PE)_2$ $(PEP)_2$ at 2% concentration of polymer in decane in a generalized Kratky representation. Effect of the molecular weight of the brush chains.

As seen in Tables 2 and 3, the average extension of the brush chains, estimated from the parameters $L$ and $\sigma_L$, for a given architecture is increased with increasing molecular weight of the arms. For the lowest molecular weight of 5000, the smearing parameter $\sigma_L$ is reduced to zero, yielding a constant density. In this case, the chains seem to be more uniformly distributed in the brush. It is interesting to note that the more the molecular weight is increased, the more an increasing $\sigma_L$ smooths the profile, leading to a significant extension of the brush chains.

Furthermore, the average thickness of the core appears to be nearly constant and independent of the molecular weight of the brush for the architecture $(PE)_2$-$(PEP)_2$, while for the architectures $(PE)(PEP)_2$ and $(PE)_2(PEP)$, this thickness decreases with increasing the molecular weight, as is also the case for PE−PEP block copolymers.[22] Figure 11 shows the effect of the molecular weight of the brush chains on the scattering intensity for the samples with architecture $(PE)_2(PEP)_2$. A slight second peak appears for the sample MAS522 at $Q \sim 0.035$ Å$^{-1}$(Figure 6), which is the fingerprint of the sharp rectangular PEP density profile in this sample and the short distance between the mass centers of the two halfs of the brush. For large molecular weight of the PEP arms, this distance is relatively large and the peak is then shifted to low $Q$ values out of the range of the instrument.

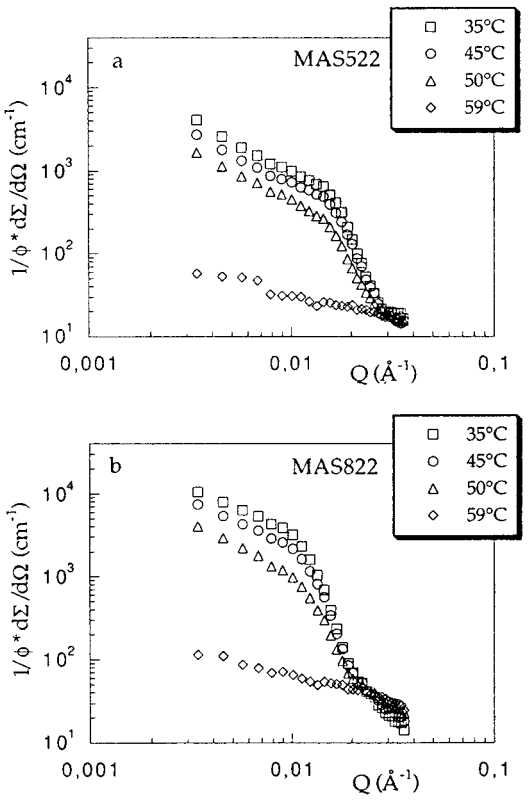


**Figure 12.** SANS cross section for samples MAS522 (a) and MAS822 (b) at 2% concentration of polymer in deuterated decane. Each curve corresponds to different temperatures.

**4.3. Influence of Architecture.** In order to discuss qualitatively the influence of the architecture, we start to compare the samples of $(PE)_2(PEP)_2$ and $(PE)_2(PEP)$ architectures. These samples differ from one another in the number of PEP arms. Tables 2 and 3 present the structural parameters of the aggregates obtained from the model fitting. It seems that for all PEP molecular weights the chains are more extended if the PE chains are connected to two PEP arms instead of one. The difference is more pronounced when the PEP molecular weights are higher. At the same time the thickness of the cores are higher for the system $(PE)_2$-(PEP).

The same is observed in terms of blob sizes $\xi$ (calculated using eq 17) which are larger for the samples with architecture $(PE)_2(PEP)$ than $(PE)_2(PEP)_2$.

We consider now the systems $(PE)_2(PEP)_2$ and (PE)-$(PEP)_2$. The average extension of the brush arms seems to be higher for the architecture $(PE)(PEP)_2$ than $(PE)_2$-$(PEP)_2$ except the samples with the medium molecular weight $M_{PEP} \sim 9000$. On the contrary, the thickness of the core and the blob size are lower for samples (PE)-$(PEP)_2$.

A more quantitative thermodynamic model is discussed in section 5.1.

**4.4. Effect of Temperature.** A more convenient method of obtaining the thermodynamic functions is to determine the critical micelle temperature (cmt), defined as a temperature above which no aggregate formation occurs. These thermodynamic functions permit one to understand, among other things, the chains solubility. Parts a and b of Figure 12 present a series of SANS intensity distributions under brush contrast for samples MAS522 and MAS822 at different temperatures varying between 35 °C and 59 °C. The concentration of the polymer in decane is fixed to 2%. While around $T = 20$ °C the forward scattering depends only slightly on temperature, the $Q$ zero intensity $d\Sigma/d\Omega$ ($Q \rightarrow 0$) decreases monotonously on heating the solution up to 50 °C. On further heating the weight fraction of micelles decreases rapidly, leading to a sudden decrease in scattering intensity at higher temperatures when the micellar state disappears.

## 5. Discussion

**5.1. Thermodynamics of Aggregation of Polymers with Architecture.** As was shown in a previous publication,[22] an understanding of the structural parameters of the micelles formed of PE−PEP diblocks could be obtained in a thermodynamic approach taking into account three contributions to the free energy of a single micelle: the folding energy of the crystalline PE core, the stretching entropy of the brush (described by a blob model), and a defect energy due to ethylene side groups of the PE chain, whose integration in the PE lamella costs significant deformation energy. The equilibrium structure is the result of the balance of enthalpic and entropic contributions to the free energy.

The various expressions for the free energy are slightly modified by the polymer architecture, leading to scaling expressions containing the indices characterizing a polymer star. We describe our system generally as $(N_{PE})_{I_{PE}}(N_{PEP})_{I_{PEP}}$. Here $N_i$ is the number of monomers and $I_i$ is the number of arms of the i-component.

Before going into the detailed description of the free energies, a general correlation inherent to the model description shall be derived. The PEP brush is described by a blob model.[25,26] In this model the blob size $\xi$ and the number $g$ of monomers in one blob are connected by the Flory exponent $\nu$ via

$$\xi \cong g^{\nu} \tag{20}$$

The polymer number density in the brush must be independent from the selected volume. If we choose a blob and the whole brush, we get

$$\frac{g}{\xi^3} = \frac{N_{PEP}}{\xi^2 L} \tag{21}$$

The combination of the two equations yields

$$\xi^{1/\nu - 1} \cong N_{PEP}/L \tag{22}$$

The identical consideration on the core density leads to

$$\frac{1}{2} 2Od = I_{PE} N_{PE} a^3 \tag{23}$$

with $2O$ being the surface per miktoarm star polymer, $d$ the core thickness, and $a$ the monomer dimension. Now the surface is shared between the hairs emanating from one star, and the area per hair defines the blob diameter: $2O = I_{PEP}\xi^2$. With $\xi$ from eq 21 and $\nu = {}^3/_5$, we get finally

$$L \cong \left(\frac{I_{PEP}}{I_{PE}}\right)^{1/3} \frac{N_{PEP}}{N_{PE}^{1/3}} d^{1/3} \tag{24}$$

Figure 13 shows this relation for the miktoarm stars. The figure shows that this relation is well fulfilled for all samples, including the block copolymers.[22] The straight line shows a slope of 1.8, which is equal to that obtained for the diblock samples. Only two points fit

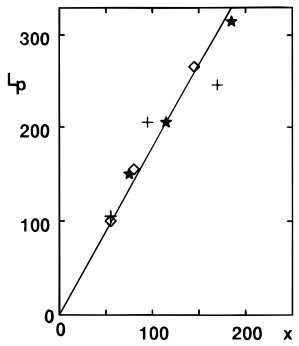


**Figure 13.** Scaling relation according to eq 24 between the average extension of the brush using a parabolic profile, $L_p$, and the core thickness, $d$. The abscissa is abbreviated $x = (I_{PEP}/I_{PE})^{1/3}(N_{PEP}/N_{PE}^{1/3})d^{1/3}$. The proportionality factor is determined by the monomer numbers $N_{PE}$ and $N_{PEP}$ of the core and the brush and the architecture factor $I_{PE}/I_{PEP}$ for miktoarm stars. The slope of the straight line is 1.8.

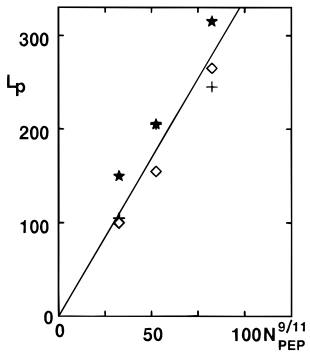


**Figure 14.** Scaling representation according to eq 30 of the average extension of the brush using a parabolic profile, $L_p$. $N_{PEP}$ is the monomer number of the brush arms for miktoarm stars. The slope of the straight line is 3.4.

badly into the general behavior. They both contain large molecular weight PEP chains. The agreement of the fit results with the outlined scaling relation means that the blob model allows a reasonable description of the PE−PEP micelles.

If the PE−PEP brushes represent equilibrium structures, then their structural parameters must emerge from a minimization of the free energy of the system. Since we are far from the cmc and the polymer fraction is almost completely condensed into the micellar phase, we can restrict the thermodynamics calculation to a single micelle. This makes the considerations simple. All free energies are calculated per miktoarm star. As the variable of our system, we choose the inverse surface area per miktoarm star in units of the monomer area $\sigma = (a^2/O)I_{PE}$. With this convention $(\sigma I_{PEP})^{-1}$ has the meaning of the grafting density.

The free energy of the brush is just the number of blobs times $k_BT$. If we call $n_{blob}$ the number of blobs per PEP arm, then we have

$$f_{PEP} \cong k_BTI_{PEP}n_{blob} = k_BTI_{PEP}N_{PEP}(a/\xi)^{5/3} \quad (25)$$

On the other hand, the PE core offers a surface $O$ per star which is shared between the emanating PEP arms such that $\xi^2 I_{PEP} = 2O$. These equations lead to a final expression of

$$f_{PEP} \cong \frac{1}{2^{5/6}}k_BT\frac{I_{PEP}^{11/6}}{I_{PE}^{5/6}}N_{PEP}\sigma^{5/6} \quad (26)$$

This conformational entropy is balanced by a crystallization energy, which besides a volume term containing the cristallization enthalpy $\Delta H$ is determined by the number $n_f$ of PE folds and the energy per fold $E_f$

$$f_{cri} = -I_{PE}N_{PE}\frac{\Delta H}{\zeta_{PE}} + I_{PE}n_fE_f \quad (27)$$

$$= c1 + I_{PE}E_f\left(\frac{1}{\sigma} - \frac{1}{I_{PE}}\right) \quad (28)$$

with $c1$ a constant independent of $\sigma$. This equation shows that the stretched chain, $\sigma = I_{PE}$, contains no folding energy.

It was found in the previous paper[22] that the ethylene side chains always attached to PE made from PB play an important role in the balance of energies. In a thick lamellae of stretched PE chains ($\sigma = I_{PE}$) all defects are incorporated into the PE lamella. This costs the maximum possible defect energy $f_{def}^0$. For a monomer thin lamella the respective energy is zero because all ethylene side chains escape to the surface and yield $f_{def} = 0$. This condition determines the value of $f_{def}^0$. This qualitative estimate can be expressed quantitatively

$$f_{def} = f_{def}^0 - I_{PE}n_spE_{def}\frac{1}{\sigma} \quad (29)$$

Here $E_{def}$ is the energy of a defect, $p$ the probability per ethylene group carrying such a side chain, and $n_s$ the distance from the surface up to which one a defect is expelled to the surface. The second term of this analytical formula follows closely a numerical calculation which determined the number of defects in a surface layer, assuming a Poisson distribution of the defects along the PE chain. The advantage of the above formulation is that it uses the specific surface as the variable and thus allows a forthgoing analytical treatment.

The total free energy is the sum of the three terms. Differentiation yields an analytically solvable equation for $\sigma$. With the resulting $\sigma_0$, we obtain the following scaling relations for the brush length

$$L \cong a\left(\frac{E'}{k_BT}\right)^{2/11}N_{PEP}^{9/11} \quad (30)$$

and the core thickness

$$d \cong a\left(\frac{E'}{k_BT}\right)^{6/11}\frac{I_{PE}}{I_{PEP}}\frac{N_{PE}^{6/11}}{N_{PEP}} \quad (31)$$

Here the primed energy means $E' = E_f - n_spE_{def}$. Thus, the brush length is expected to be independent of polymer architecture and increase with increasing the molecular weight of the PEP arm. It is only the properties of the single arm which enter. The core thickness, on the other hand, depends on all parameters characterizing the star polymer. With respect to the PE part there is no difference whether a single arm is doubled in mass or whether a second short arm is added to the star. In its effect on the brush, however, a doubling of the arms has a larger effect than a doubling of the mass of one arm.

Figures 14 and 15 show the respective scaling representations for miktoarm stars. The scaling variables are derived from Table 1. To allow a comparison with the parameters of the parabolic profiles of the brush used in the presentation of the data of the previous

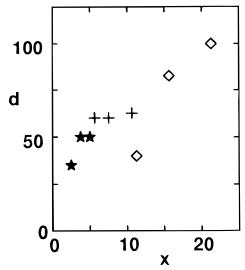


**Figure 15.** Scaling representation according to eq 31 of the core thickness $d$ for the samples with the monomer numbers $N_{PE}$ and $N_{PEP}$ of the core and the brush arms and the architecture factor $I_{PE}/I_{PEP}$ for miktoarm stars. $x = (I_{PE}/I_{PEP})(N_{PE}/N_{PEP}^{6/11})$.

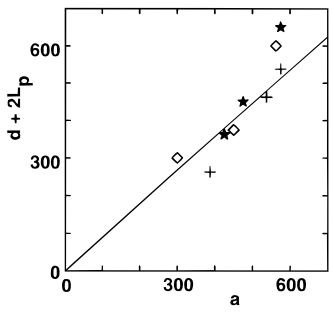


**Figure 16.** Total thickness ($d + 2(L_p)$) of the platelets against the intermicellar distance $a$ for miktoarm star polymers.

publication,[22] the smeared step profiles of the PEP density were fitted in the range from the maximum density at the PE−PEP interface up to a distance where this density has decreaced by a factor 10 by a parabola. As the brush length, the intersection of the parabola with the abscissa, $L_p$ (Table 2), is taken. Based on these values, the brush length follows reasonably well the predictions of the scaling and the slope is almost the same as that obtained for the diblocks, 3.44.[22] The core thickness, on the other hand, shows systematic deviations from the expected scaling. While the PEP rich three-arm stars follow a linear relationship the PE-rich system is more erratic. The four-arm stars show an almost constant core thickness. Altogether it looks as if the core thickness would be independent of the number of PE arms. This is in clear contradiction to the estimated effect of polymer architecture. It is very astonishing that the stars with architecture behave so differently compared to the block copolymers. (It must be mentioned, however, that the diblocks investigated by Lin and Gast[23] by SAXS also do not obey the $d$-scaling relation.) If deviations from scaling behavior would be due to an inaccurate knowledge of the sample parameters, erroneous points should appear in the series of samples since all stars were prepared from the same fraction of polymer arms. This is not the case. However, if the micellar shapes would be controlled by the kinetics of aggregation, that is if the micelles do not represent equilibrium structures at room temperature, then any result is possible. This is very unlikely, however, since the samples were prepared according to identical heat treatment.

The outlined inconsistency is on the order of a factor 2. Motivated by the success of the model with diblocks, we try to get quantitative results from the slopes of the two scaling relations, too. This slope is in both cases related to $E'$ in units of $k_BT$. The final result is

$$E' = 1.83k_BT \qquad (32)$$

A variety of sample parameters determines $E'$ (see above). Since PE is one of the best known polymers, most of the required quantities can be found in the literature. The folding energy of a PE chain amounts typically to $E_f \sim 170$ meV. Further the probability for a ethylene side chain is $p = 0.018$ for a PE synthesized by hydrogenation of (1−4)PB. Finally, an approximate value of the defect energy was obtained recently in a systematic study of a the crystallization enthalpy of various PE materials containing an increasing number of ethylene side chains. The change in crystallization energy was attributed to the defect energy which happened to be $E_{def} \sim 600$ meV.[34] This looks reasonable in comparison to the fold energy because a defect forces a PE chain to make a small number of folds around it. Correspondingly, the defect energy should be a few times the fold energy. Thus, the only unknown of the equation becomes $n_s \sim 11$. This number compares favorably with the value $n_s = 14$ obtained for diblocks.[22] The related PE chain length amounts to ∼14 Å. Due to the random distribution of the ethylene defects along the carbon backbone, a tendency of excluding defects is directly related to a surface roughness. Very likely the large values $\sigma_d$ (Table 2 and 3) are due to this effect.

In the most simple approach to the free energy[19] the defect energy is not considered. The scaling relations do not change in this case because both the folds and the defects show the same dependence on the grafting density $\sigma$. However, the slopes of the scaling relations need a different interpretation. Neglecting the defects makes in our formalism $E' \sim E_f$, which is in severe contradiction with the known value of $E_f = 170$ meV.

**5.2. Micellar Aggregation.** After having discussed the shape of a single micelle and the underlying thermodynamics, we have to find a reason for the aggregation of micelles. It was shown in the previous paper[22,24] that one can consider the system of micelles as a free gas. If they aggregate, they lose entropy. Thus, there must be an attractive interaction to counterbalance this loss. This is the van der Waals (vdW) interaction between parallel platelets. In a two-dimensional object the vdW interaction increases with the inverse square of the interlamellar distance and thus exceeds at short enough interlamellar distances the entropic repulsion. There is no effect of architecture in these considerations, and all the semiquantitative estimates can be found in ref 22. Since the vdW interaction becomes efficient only at short distances of the micelles we expect a correlation between the geometrical parameters of the single micelle and the intermicellar distance. In Figure 15 we have plotted the total thickness of a micelle ($d + 2L_p$) against the intermicellar distance $a$.

Indeed the data points are all close to a straight line, which again is close to $(d + 2L_p) = a$. A problem consists of a reasonable choice of the brush length. The model of the box profile smeared by a Gaussian does not yield a sharp value. The sharp surface when working with a parabolic profile is unrealistic also. Thus, no more detailed information can be extracted.

## 6. Summary and Conclusions

The aggregation behavior of miktoarm star polymers $(PE)_n(PEP)_m$ with $n, m \leq 2$ and $n + m = 3,4$ dissolved in the selective solvent decane was investigated by small-angle neutron scattering as a function of the length of the PEP arms and the polymer architecture using the contrast variation technique. For the latter

purpose the PE arms were partially deuterated and the PEP arms fully protonated, while the degree of deuteration of the solvent was varied in the range of the corresponding scattering length densities. A 2% polymer concentration was chosen.

Like in the case of PE−PEP diblocks,[22] the SANS patterns show the signature of lamellar micelles consisting of a chain-folded inner PE lamella separated from the solvent by solvated amorphous PEP brushes. By model fitting, the structural parameters characterizing the platelets have been extracted. The density profiles of the core and the corona were described by step functions smoothed by convolution with a Gaussian each. We find that the platelets are laterally greatly extended and model them as disks of a diameter $2R \geq 12\,000$ Å, a size which causes no features in the experimental range. The flat dense crystalline PE core shows thicknesses between 35 and 96 Å, while the length of the surrounding PEP hairs increases with the molecular weight and increasing number of arms of PEP from 100 to 300 Å.

The equilibrium properties of the polymer brushes can be derived by a thermodynamic approach which yields structural parameters for different molecular weights and architectures. Due to the low solubility of the polymers at room temperature, a free energy expression for a single micelle, used successfully in the case of diblocks,[22] was generalized for the miktoarm star with architecture. The relevant energies are the chain-folding enthalpy of the crystalline PE core and a defect energy due to the incorporation of ethylene side chains on the one hand, which, on the other hand, are balanced by the deformation entropy of the tethered PEP arms. The latter is described by a blob model.[25,26] It is important to note that the structures of the brushes and the crystalline blocks depend on one another through the chemical bond between them. The minimization of this free energy yields a number of scaling relations. While the brush length is in reasonable agreement with the thermodynamic model, the core thickness scatters by a factor 2 around the scaling behavior. The average description of the data by the thermodynamic model yields reasonable values of the fold and defect energies.

On a larger scale van der Waals interaction between large micelles leads to macroaggregates of finite size in the micron regime which can be observed directly in the light microscope under phase contrast.

Finally, some data on the temperature dependence of the aggregates were taken. A critical micelle temperature (cmt) of about 60 °C was found.

**Acknowledgment.** This research was supported by the European community under the Brite Euram Contract BRE2-CT93−0454. We are grateful to T. C. B. McLeish of Leeds University for fruitful discussions. We thank the Laboratoire Léon Brillouin (LLB) and Institut Laue-Langevin (ILL), for providing us the SANS beam time. Helpful discussions with F. Boué of LLB, P. Lindner of ILL and W. Pyckhout of KFA are appreciated as well as the technical assistance during the SANS measurements. We thank L. Willner for polymer hydrogenation.

## References and Notes

(1) Halperin, A.; Tirell, M.; Lodge, T. P. *Adv. Polym. Sci.* **1992**, *100*, 31.
(2) Gast, A. P. *Scientific Methods for the Study of Polymer Colloids and Their Applications*; Kluwer Academic Publishers: Dordrecht, The Netherlands, 1990; pp 311−328.
(3) Tuzur, Z.; Kratochvil, P. *Advances in Colloid and Interface Science*; Elsevier: Amsterdam, The Netherlands, 1976.
(4) Higgins, J. S.; Dawkins, J. V.; Maghami, G. G.; Shakir, S. A. *Polymer* **1986**, *27*, 931.
(5) Plestil, J.; Baldrian, *J. Makromol. Chem.* **1975**, *176*, 1009.
(6) Bluhm, T. L.; Malhorta, S. L.; Hong, M.; Noolandi, J. *Polym. Prepr. Am. Chem. Soc., Div. Polym. Chem.* **1983**, *24*, 405.
(7) Oranli, L.; Bahadur, P.; Riess, G. *Can. J. Chem.* **1985**, *63*, 2691.
(8) Bahadur, P.; Sastry, N. V.; Marti, S.; Riess, G. *Colloids Surf.* **1985**, *16*, 337.
(9) Gallot, Y.; Franta, P.; Rempp, P.; Benoit, H. *J. Polym. Sci., Part C* **1964**, *4*, 473.
(10) Kotaka, T.; Tanaka, T.; Hattori, M.; Inagaki, H. *Macromolecules* **1978**, *11*, 138.
(11) Periard, J.; Riess, G. *Eur. Polym. J.* **1973**, *9*, 687.
(12) Selb, J.; Gallot, Y. *Makromol. Chem.* **1980**, *182*, 1491.
(13) Alward, D. B.; Kinning, D. J.; Thomas, E. L.; Lewis, L. J. *Macromolecules* **1986**, *19*, 215.
(14) Perret, R.; Skoulious, A. *Makromol. Chem.* **1972**, 162, *147*, 163.
(15) Gervais, M.; Gallot, B. *Makromol. Chem.* **1973**, *171*, 157.
(16) Gervais, M.; Gallot, B. *Makromol. Chem.* **1977**, *178*, 1577; **1977**, *178*, 2071.
(17) Lotz, B.; Kovacs, A. A. *Polym. Prepr. (Am. Chem. Soc., Div. Polym. Chem.)* **1969**, *10*, 820.
(18) Hayashi, T. In *Developments in Block Copolymers−2*; Ed.; Goodman, I. Elsevier Applied Science: London, **1985**; Chapter 4.
(19) Vilgis, T.; Halperin, A. *Macromolecules* **1991**, *24*, 2090.
(20) DiMarzio, E. A.; Guttman, C. M.; Hoffmann, J. D. *Macromolecules* **1980**, *13*, 1194.
(21) Whitmore, M. D.; Noolandi, J. *Macromolecules* **1988**, *21*, 1482.
(22) Richter, D.; Schneiders, D.; Monkenbusch, M.; Willner, L.; Fetters, L. J.; Huang, J. S.; Lin, M.; Mortensen, K.; Farago, B. *Macromolecules* **1997**, in press.
(23) Lin, E. K.; Gast, A. P.; *Macromolecules* **1996**, *29*, 4432.
(24) Schneiders, D. Thesis, Aachen University, Aachen, Germany, 1996.
(25) Alexander, S. J. *Phys.* **1977**, *38*, 983.
(26) de Gennes, P.-G. *Macromolecules* **1980**, *13*, 1069.
(27) Milner, S. T.; Witten, T. A.; Cates, M. E. *Macromolecules* **1988**, *21*, 2610.
(28) Bates, R.; Rosedale, J.; Bair, H.; Russell, T. *Macromolelcules* **1989**, *22*, 2557.
(29) Iatrou, H.; Hadjichristidis, N. *Macromolecules* **1992**, *25*, 4649.
(30) Allgaier, J.; Young, R. N.; Efstratiadis, V.; Hadjichristidis, N. *Macromolecules* **1995**, *29*, 1794.
(31) Iatrou, H.; Hadjichristidis, N. *Macromolecules* **1993**, *26*, 2479.
(32) Iatrou, H; Siakali-Kioulafa, E.; Hadjichristidis, N.; Roovers, J.; Mays, J. *J. Polym. Sci., Polym. Phys.* **1995**, *33*, 1925.
(33) Tanzer, J. D.; Bartels, C. R.; Christ, B.; Graessley, W. W. *Macromolecules* **1984**, *17*, 2708.
(34) Gaucher, V.; Séguéla, R. *Polymer* **1994**, *35*, 2049.
(35) Crist, B.; Nicholson, J. C. *Polymer* **1994**, *35*, 1846.
(36) Higgins, J. S.; Benoit, H. In *Polymers and Neutrons Scattering*; Clarendon Press: Oxford, U.K., 1994.
(37) Cotton, J. P. In *Neutron, X-Ray and Light Scattering*; Lindner, P., Zemb, T., Eds.; Elsevier: Amsterdam, The Netherlands, 1991.
(38) Feigin, L. A.; Svergun, D. I. *Structure analysis by small-angle X-ray and neutron scattering*; Taylor, G. W., Ed.; Plenum Press: New York, 1887.
(39) Guinier, A.; Fournet, G. *Small angle scattering of X-ray.*; Wiley: New York, 1955.
(40) Hosemann, R.; Bagchi, S. N. *Direct Analysis of Diffraction by Matter*; North-Holland: Amsterdam, The Netherlands, 1962.
(41) Dozier, W. D.; Huang, J. S.; Fetters, L. J. *Macromolecules* **1991**, *24*, 2810.
(42) Pedersen, J. S.; Posselt, D.; Mortensen, K. *J. Appl. Crystallogr.* **1990**, *23*, 321.

MA9700385